Polyhedron 30 (2011) 61–69

Contents lists available at ScienceDirect

Polyhedron

journal homepage: www.elsevier.com/locate/poly

Electronic and steric effects of substituents on the conformational diversity and hydrogen bonding of *N*-(4-X-phenyl)-*N*′,*N*″-bis(piperidinyl) phosphoric triamides (X = F, Cl, Br, H, CH_3): A combined experimental and DFT study

Khodayar Gholivand *, Hamid Reza Mahzouni

Department of Chemistry, Tarbiat Modares University, P.O. Box 14115-175, Tehran, Iran

ARTICLE INFO

Article history:
Received 6 July 2010
Accepted 23 September 2010
Available online 4 November 2010

Keywords:
Conformer
DFT calculation
Hydrogen bond
Phosphoric triamide
X-ray crystallography

ABSTRACT

Phosphoric triamides of the general formula (4-X-C_6H_4NH)P(O)($NC_5H_{10})_2$, X = F (**1**), Cl (**2**), Br (**3**), H (**4**) and CH_3 (**5**), have been synthesized and characterized. X-ray crystallography at 120 K reveals that the compounds **1**, **3**, **4**·$\mathbf{H_2O}$ and **5** are composed of one, four, two and four conformers, respectively. DFT calculations were performed to investigate the electronic structures of the compounds. The X-ray data and DFT calculations revealed that the conformational diversity in these compounds is mainly governed by the steric effects of the substituent X rather than by electronic effects. Although substituent X does not participate directly in hydrogen bonding, the crystal packing of the compounds is influenced by the size of X. Atoms in molecules (AIM) and natural bond orbital (NBO) analyses confirm that the *para* substituent X has no significant effect on the electronic features of the amidic proton and the phosphoryl oxygen atom (O_P). Using X-ray crystallography, AIM and NBO analyses, the structural and electronic aspects of inter- and intramolecular hydrogen bonds of the compounds have been studied. The charge density (ρ) at the bond critical point (bcp) of the N–H bond decreases from the fully optimized monomers to their corresponding hydrogen bonded clusters. The N–H stretching frequency decreases from the calculated values to the experimental results.

1. Introduction

Phosphoric triamides have received considerable attention due to their applications as inhibitors of urease [1–3] and acetylcholinesterase [4,5] and as stereoselective catalysts [6–8]. Furthermore, we have already shown that phosphoric triamides can be considered as an efficient extracting agent for lanthanides [9]. The ring inversion and rotation of cyclic amines around the P–N bond provide different conformers in phosphoric triamides [10,11]. Such compounds with two [12–14], three [15,16] and four [17,18] conformers have been previously reported. The conformational diversity in these compounds creates a wide range of hydrogen bonds [17,18]. It is well known that hydrogen bonds play a key role in biochemical processes such as enzymatic activity [19,20] and protein–ligand interactions [21]. Moreover, physicochemical properties of compounds (boiling and melting points, density, dipole moment, etc.) depend on the presence of non-covalent interactions and intermolecular hydrogen bonds [22]. Hence, the analysis of hydrogen bonds is helpful to rationalize the structural and physicochemical properties of compounds. In previous works, we have performed conformational analysis of phosphoric triamides with three [16] and four conformers [17]. In this area, a comparison of the electronic and steric effects of substituents on the structure of conformers needs to be investigated. The major aim of the present work is to investigate which of the electronic or steric effects can influence the formation of various conformers. In the present study, five compounds with the formula (4-X-C_6H_4NH)P(O)($NC_5H_{10})_2$, X = F (**1**), Cl (**2**), Br (**3**), H (**4**) and CH_3 (**5**) have been synthesized and characterized. The solid state structures of compounds **1** and **3**–**5** were determined by X-ray crystallography. The compounds **1**, **3**, **4**·$\mathbf{H_2O}$ and **5** contain one, four, two and four conformers, respectively, in the solid phase. The X-ray structures were employed as references for quantum mechanical (QM) calculations at the B3LYP level. The electronic features of the hydrogen bonds were investigated by Natural Bonding Orbital (NBO) and Atoms in Molecules (AIM) analyses to rationalize the structural and physicochemical properties of the compounds. Moreover, infrared spectroscopy was used to get a more detailed insight into the structure of the hydrogen bonds.

2. Experimental

2.1. Instrumentation

^1H, ^{13}C and ^{31}P spectra were recorded on a Bruker Avance DRX 500 spectrometer. ^1H and ^{13}C chemical shifts were determined

* Corresponding author. Tel.: +98 21 82883443; fax: +98 21 8006544.
E-mail address: gholi_kh@modares.ac.ir (K. Gholivand).

0277-5387/$ - see front matter Crown Copyright © 2010 Published by Elsevier Ltd. All rights reserved.
doi:10.1016/j.poly.2010.09.039

relative to internal TMS, and ^{31}P chemical shifts relative to 85% H_3PO_4 as an external standard. Infrared (IR) spectra were recorded on a Shimadzu model IR-60 spectrometer using KBr pellets. Melting points were obtained with an Electrothermal instrument. Single crystals of the compounds **1**, **3**, **4·H$_2$O** and **5** were obtained from a mixture of CH_3OH/H_2O at room temperature. X-ray data were collected on a Bruker SMART area detector [23] single crystal diffractometer with graphite monochromated Mo Kα radiation (λ = 0.71073 Å). All the structures were refined by full-matrix least-squares methods against F^2 with SHELXL-97 [24]. Routine Lorentz and polarization corrections were applied and an absorption correction was performed using the SADABS program [25] for compounds **3**, **4·H$_2$O** and **5**. The crystallographic data of compounds **1**, **3**, **4·H$_2$O** and **5** are summarized in Table 1.

2.2. General procedure for the synthesis of compounds *1–5*

The intermediates (4-X-C_6H_4NH)P(O)Cl_2 (X = F, Cl, Br, H and CH_3) were prepared according to the literature procedures [26]. Then, a solution of 4 mmol piperidine in dry acetonitrile (30 ml) was added dropwise to a stirred solution of 1 mmol (4-X-C_6H_4NH)P(O)Cl_2 at −5 °C. After 5 h stirring, the solvent was evaporated under vacuum. The resulting white product was washed with distilled water and recrystallized from a mixture of methanol and water.

2.3. N-4-fluorophenyl-N′,N″-bis(piperidinyl) phosphoric triamide (*1*)

Yield: 78%, m.p. 199 °C. ^1H NMR ($CDCl_3$, 500.13 MHz, 298 K): 1.43 (m, 8H, CH_2), 1.50 (m, 4H, CH_2), 3.10 (m, 8H, CH_2), 4.76 (d, ^2J(PNH) = 7.0 Hz, 1H, NH), 6.88 (m, 2H, Ar-H), 7.02 (m, 2H, Ar-H) ppm. $^{13}C\{^1H\}$ NMR ($CDCl_3$, 125.76 MHz, 298 K): 26.58 (s, CH_2), 26.28 (d, ^3J(P,C) = 5.2 Hz, CH_2), 45.73 (d, ^2J(P,C) = 2.2 Hz, CH_2), 115.49 (d, ^2J(F,C) = 22.4 Hz), 119.30 (m, ^3J[(F,C), (P,C)] = 6.9 Hz), 137.33 (s), 157.71 (d, ^1J(F,C) = 239.1 Hz) ppm. $^{31}P\{^1H\}$ NMR ($CDCl_3$, 202.46 MHz, 298 K): 12.57 (s) ppm. $^{31}P\{^1H\}$ NMR (acetone-d_6, 162.01 MHz, 190 K): 10.58 (s) ppm. IR (KBr, cm^{-1}): 3180, 2930, 2820, 1602, 1501, 1437, 1379, 1332, 1280, 1208, 1185, 1066, 1024, 952, 929, 827, 716, 677, 550, 482.

2.4. N-4-chlorophenyl-N′,N″-bis(piperidinyl) phosphoric triamide (*2*)

Yield: 60%, m.p. 191 °C. ^1H NMR ($CDCl_3$, 500.13 MHz, 298 K): 1.44 (m, 8H, CH_2), 1.54 (m, 4H, CH_2), 3.05 (m, 8H, CH_2), 5.06 (d, ^2J(PNH) = 7.2 Hz, 1H, NH), 7.02 (d, ^3J(H,H) = 8.6 Hz, 2H, Ar-H), 7.14 (d, ^3J(H,H) = 8.6 Hz, 2H, Ar-H) ppm. $^{13}C\{^1H\}$ NMR ($CDCl_3$, 125.76 MHz, 298 K): 22.45 (s, CH_2), 26.27 (d, ^3J(P,C) = 5.0 Hz, CH_2), 45.71 (d, ^2J(P,C) = 2.1 Hz, CH_2), 119.13 (d, ^3J(P,C) = 6.3 Hz, C_{ortho}), 125.88 (s), 128.93 (s), 140.04 (s) ppm. $^{31}P\{^1H\}$ NMR ($CDCl_3$, 202.46 MHz, 298 K): 12.33 (s) ppm. $^{31}P\{^1H\}$ NMR (acetone-d_6, 162.01 MHz, 190 K): 10.45 (s) ppm. IR (KBr, cm^{-1}): 3188, 2930, 1504, 1486, 1437, 1375, 1331, 1233, 1207, 1160, 1066, 951, 933, 718, 634, 556, 497.

2.5. N-4-bromophenyl-N′,N″-bis(piperidinyl) phosphoric triamide (*3*)

Yield: 73%, m.p. 197 °C. ^1H NMR ($CDCl_3$, 500.13 MHz, 298 K): 1.45 (m, 8H, CH_2), 1.55 (m, 4H, CH_2), 3.11 (m, 8H, CH_2), 4.76 (d, ^2J(PNH) = 5.4 Hz, 1H, NH), 6.96 (d, ^3J(H,H) = 8.6 Hz, 2H, Ar-H), 7.30 (d, ^3J(H,H) = 8.6 Hz, 2H, Ar-H) ppm. ^1H NMR (acetone-d_6, 400.22 MHz, 190 K): 1.44 (b, CH_2), 1.54 (b, CH_2), 3.09 (b, CH_2), 6.92 (b, Ar-H), 7.20 (b, Ar-H) ppm. $^{13}C\{^1H\}$ NMR ($CDCl_3$, 125.76 MHz, 298 K): 24.58 (s, CH_2), 26.31 (d, ^3J(P,C) = 5.0 Hz, CH_2), 45.78 (d, ^2J(P,C) = 1.2 Hz, CH_2), 113.32 (s), 119.50 (d, ^3J(P,C) = 6.3 Hz, C_{ortho}), 131.95 (s), 140.50 (s) ppm. $^{31}P\{^1H\}$ NMR ($CDCl_3$, 202.46 MHz, 298 K): 12.20 (s) ppm. $^{31}P\{^1H\}$ NMR (acetone-d_6, 162.01 MHz, 190 K): 10.48 (s) ppm. IR (KBr, cm^{-1}): 3140,

Table 1
Crystallographic data for compounds **1** and **3–5**.

	1	**3**	**4·H$_2$O**	**5**
Empirical formula	$C_{16}H_{25}FN_3OP$	$C_{16}H_{25}BrN_3OP$	$C_{32}H_{54}N_6O_3P_2$	$C_{17}H_{28}N_3OP$
Formula weight	325.36	386.26	632.75	321.39
Temperature (K)	120(2)	120(2)	120(2)	120(2)
Wavelength (Å)	0.71073	0.71073	0.71073	0.71073
Crystal system, space group	Monoclinic, $P2_1/c$	Triclinic, $P\bar{1}$	Triclinic, $P\bar{1}$	Triclinic, $P\bar{1}$
Unit cell dimensions				
a (Å)	10.0001(11)	14.321(7)	12.106(3)	14.2998(10)
b (Å)	16.9181(18)	16.291(8)	12.548(3)	16.2595(11)
c (Å)	10.0303(11)	16.574(8)	12.650(3)	16.6649(12)
α (°)	90	73.986(10)	111.627(5)	73.878(10)
β (°)	99.805(2)	71.566(9)	96.733(5)	71.618(10)
γ (°)	90	80.593(10)	106.243(5)	81.295(10)
V (Å^3)	1696.8(3)	3514(3)	1700.6(7)	3523.7(5)
Z, D_{calc} (mg m^{-3})	4, 1.274	8, 1.460	2, 1.236	8, 1.212
Absorption coefficient (mm^{-1})	0.177	2.422	0.169	0.162
F(0 0 0)	696	1600	684	1392
Crystal size (mm)	0.35 × 0.15 × 0.10	0.10 × 0.10 × 0.05	0.22 × 0.18 × 0.17	0.35 × 0.24 × 0.20
θ Range for data collection (°)	2.04–28.07	1.63–26.02	1.77–26.00	1.31–25.00
Limiting indices				
	$-13 \le h \le 13$ $-22 \le k \le 12$ $-13 \le l \le 12$	$-17 \le h \le 17$ $-20 \le k \le 19$ $-20 \le l \le 20$	$-14 \le h \le 14$ $-12 \le k \le 15$ $-14 \le l \le 15$	$-17 \le h \le 12$ $-19 \le k \le 14$ $-19 \le l \le 19$
Reflections collected/unique	11704/4063 [R_{int} = 0.0438]	27603/12998 [R_{int} = 0.0584]	10874/6621 [R_{int} = 0.0326]	17884/12124 [R_{int} = 0.0370]
Completeness to θ	98.4%	93.8%	98.8%	97.8%
Refinement method	Full-matrix least-squares on F^2	Full-matrix least-squares on F^2	Full-matrix least-squares on F^2	Full-matrix least-squares on F^2
Data/restraints/parameters	4063/0/199	12998/6/793	6621/0/428	12124/0/797
Goodness-of-fit on F^2	1.006	1.064	1.062	1.002
Final R indices	R_1 = 0.0520, wR_2 = 0.1165	R_1 = 0.0809, wR_2 = 0.1929	R_1 = 0.0668, wR_2 = 0.1301	R_1 = 0.0494, wR_2 = 0.0840
R indices (all data)	R_1 = 0.0789, wR_2 = 0.1308	R_1 = 0.1188, wR_2 = 0.2025	R_1 = 0.1044, wR_2 = 0.1445	R_1 = 0.1098, wR_2 = 0.0934
Largest difference in peak and hole (e Å^{-3})	0.390 and −0.297	4.651 and −1.186	0.348 and −0.364	0.301 and −0.357

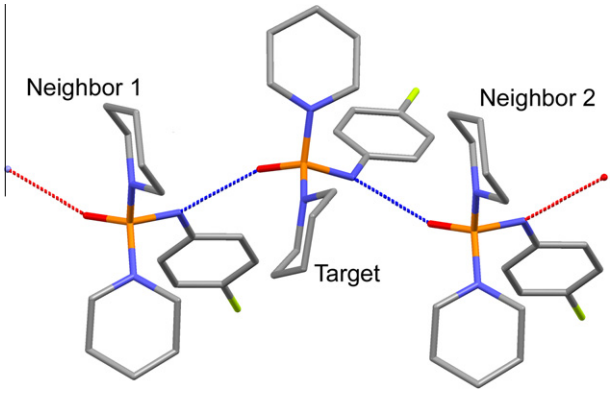

Fig. 1. The model cluster of compound **1** for DFT calculations, in which the target molecule is in the center. A similar model was also used for the other compounds.

2930, 1584, 1480, 1437, 1377, 1333, 1295, 1207, 1155, 1066, 951, 923, 720, 630, 558, 495.

2.6. N-phenyl-N′,N″-bis(piperidinyl) phosphoric triamide, (*4*)

Yield: 82%, m.p. 128 °C. The spectroscopic data are represented for the water adduct **4·H₂O**. ^{1}H NMR ($CDCl_3$, 500.13 MHz, 298 K): 1.45 (m, 8H, CH_2), 1.53 (m, 4H, CH_2), 3.10 (m, 8H, CH_2), 4.70 (d, ^2J(PNH) = 6.9 Hz, 1H, NH), 6.88 (t, ^3J(H,H) = 7.6 Hz, 1H, Ar-H), 7.03 (d, ^3J(H,H) = 7.6 Hz, 2H, Ar-H), 7.19 (t, ^3J(H,H) = 7.6 Hz, 2H, Ar-H), 7.25 (b, H_2O) ppm. ^{13}C{^{1}H} NMR ($CDCl_3$, 125.76 MHz, 298 K): 24.60 (s, CH_2), 26.28 (d, ^3J(P,C) = 5.2 Hz, CH_2), 45.75 (d, ^2J(P,C) = 2.3 Hz, CH_2), 117.87 (d, ^3J(P,C) = 6.3 Hz, C_{ortho}), 120.97 (s), 129.04 (s), 141.20 (s) ppm. ^{31}P{^{1}H} NMR ($CDCl_3$, 202.46 MHz, 298 K): 12.51 (s) ppm. ^{31}P{^{1}H} NMR (acetone-d_6, 162.01 MHz, 190 K): 10.46 (s) ppm. IR (KBr, cm^{-1}): 3450, 3145, 2925, 1593, 1488, 1437, 1376, 1286, 1210, 1170, 1066, 952, 926, 743, 717, 688, 548, 481.

2.7. N-4-methylphenyl-N′,N″-bis(piperidinyl) phosphoric triamide (*5*)

Yield: 77%, m.p. 177 °C. ^{1}H NMR ($CDCl_3$, 500.13 MHz, 298 K): 1.44 (m, 8H, CH_2), 1.51 (m, 4H, CH_2), 2.22 (s, 3H, CH_3), 3.08 (m, 8H, CH_2), 4.67 (d, ^2J(PNH) = 7.1 Hz, 1H, NH), 6.92 (d, ^3J(H,H) = 8.2 Hz, 2H, Ar-H), 6.98 (d, ^3J(H,H) = 8.2 Hz, 2H, Ar-H) ppm. ^{1}H NMR (acetone-d_6, 400.22 MHz, 190 K): 1.45 (b, CH_2), 1.53 (b, CH_2), 2.23 (s, CH_3), 3.11 (b, CH_2), 6.98 (b, Ar-H), 7.15 (b, Ar-H) ppm. ^{13}C{^{1}H} NMR ($CDCl_3$, 125.76 MHz, 298 K): 20.52 (s, *p*-CH_3), 24.63 (s, CH_2), 26.30 (d, ^3J(P,C) = 5.0 Hz, CH_2), 45.75 (d, ^2J(P,C) = 2.0 Hz, CH_2), 117.98 (d, ^3J(P,C) = 6.0 Hz), 129.50 (s), 130.14 (s), 138.62 (s) ppm. ^{31}P{^{1}H} NMR ($CDCl_3$, 202.46 MHz, 298 K): 12.62 (s) ppm. ^{31}P{^{1}H} NMR (acetone-d_6, 162.01 MHz, 190 K): 10.59 (s) ppm. IR (KBr, cm^{-1}): 3150, 2825, 1686, 1505, 1437, 1378, 1279, 1210, 1187, 1065, 951, 929, 808, 574, 467.

2.8. Computational details

The X-ray structures were used as starting points for DFT calculations in the gas phase. The structures were modelled as clusters in which the target molecule is surrounded by two neighbors (Fig. 1). Since X-ray crystallography cannot locate accurately the position of the hydrogen atoms, optimization of the hydrogen atoms positions is needed for the X-ray structures. The B3LYP/6-31G* level of theory was used to optimize only the hydrogen atom positions in the clusters, while other atoms were kept frozen during the process. The electronic features of the optimized clusters were studied by NBO [27] and AIM analyses at the B3LYP/6-31+G* level. The AIM analysis was performed by means of the Bader's Atoms in Molecules methodology [28,29]. Moreover, the monomers **1**–**5** were fully optimized in a vacuum at the B3LYP/6-31G* level. Then, the stretching frequencies, NBO charges and charge densities of the optimized monomers were calculated at the B3LYP/6-31+G* level. The geometry and electronic features of the monomers **1** and **3**–**5** were compared with those of clusters. All quantum chemical calculations have been carried out using the Gaussian 98 package [30].

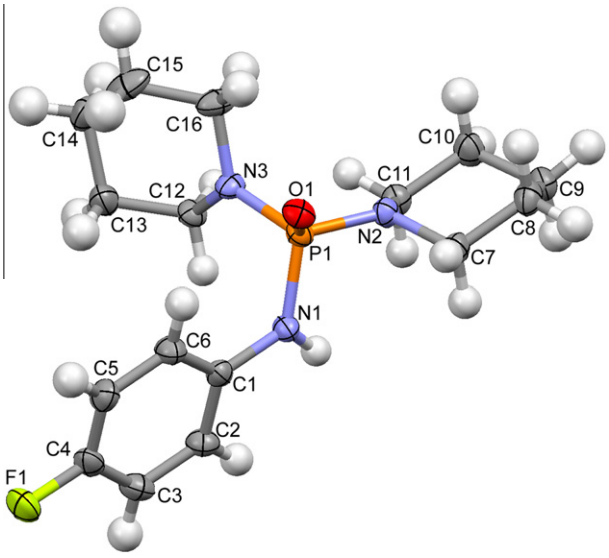

Fig. 2. Thermal ellipsoids of **1** at 50% probability.

3. Results and discussion

3.1. Spectroscopic investigation

The spectroscopic data of compounds **1**–**5** are summarized in Table 2. The IR spectra of compounds **1** and **2** show sharp bands at 3180 and 3188 cm^{-1}, respectively. This indicates that the N–H bonds are involved in one type of hydrogen bond. The IR spectra of compounds **3**, **4·H₂O** and **5** show wide bands for the N–H stretching frequency, because the various conformers are involved in different, strong or weak hydrogen bonds.

In the IR spectra, the P=O stretching frequency changes from 1155 to 1187 cm^{-1}, while the values of 1235 or 1236 cm^{-1} were calculated for the P=O vibration in all of the optimized monomers.

Table 2
Spectroscopic data of compounds **1**–**5** with the formula (4-X-C_6H_4NH)P(O)(NC_5H_{10})$_2$.

Compound	$\delta(^{31}P)$ (ppm)	$^2J_{PNH}$ (Hz)	$^{2,3}J(P,C)_{aliphatic}$ (Hz)	$^3J(P,C)_{aromatic}$ (Hz)	ν(P=O)	ν(N–H)	$\nu(P–N)_{aromatic}$
1	12.57	7.0	2.2, 5.2	6.9	1185	3180 (s)	929
2	12.33	7.2	2.1, 5.0	6.3	1160	3188 (s)	933
3	12.20	5.4	1.2, 5.0	6.3	1155	3140 (w)	923
4·H₂O[a]	12.51	6.9	2.3, 5.2	6.3	1170	3145 (w)	926
5	12.62	7.1	2.0, 5.0	6.0	1187	3150 (w)	929

[a] The spectroscopic data are represented for the water adduct, **4·H₂O**, that contains two conformers **4a**, **4b** and one water molecule.

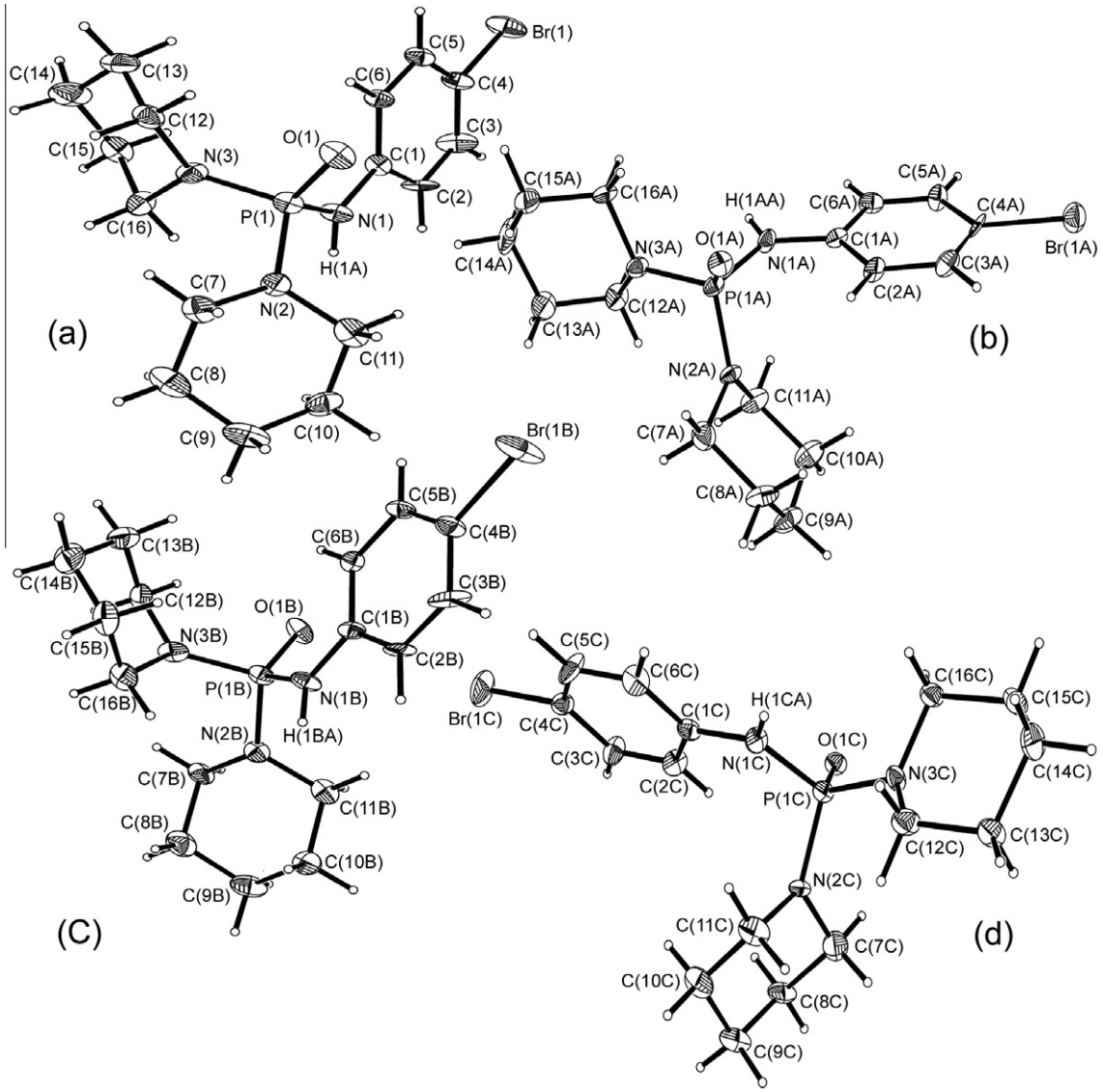

Fig. 3. Thermal ellipsoids (at the 50% probability level) of four conformers **3a** (a), **3b** (b), **3c** (c) and **3d** (d).

This difference can be attributed to hydrogen bonding in the solid phase.

Using IR and NMR spectroscopy and X-ray crystallography, we have previously shown that N-benzoyl-N′,N″-bis(*tert*-butyl) phosphoric triamide, $C_6H_4C(O)NHP(O)(NHC_4H_9)_2$, contains two conformers in both solution and the solid state [12]. Herein, the NMR spectra cannot explain the conformational diversity of the titled compounds. The $^{31}P\{^1H\}$NMR spectra at 298 K show a single resonance in all compounds **1**–**5**. The phosphorus chemical shift varies from 12.20 to 12.62 ppm and $^2J_{PNH}$ coupling constants are in the range 5.4–7.2 Hz. Thus, it can be concluded that the *para* substituent of aniline has no significant effect on the chemical environment of the P–N–H moiety. In order to investigate the conformational variety of compounds **1**–**5** in solution, low temperature NMR experiments were performed. The $^{31}P\{^1H\}$NMR spectra at 190 K show also a single resonance in all compounds **1**–**5** indicating that these compounds present only one conformer in solution. A slight decrease is seen in the phosphorus chemical shifts for the low temperature experiments, probably due to the general solvent or temperature effects. The ^1H NMR data obtained at 190 K are not able to determine whether the compounds show more conformers at low temperatures, because the peaks in the ^1H NMR spectra are shortened and broadened when the temperature is decreased in line with the decrease in solubility of the compounds. This makes the ^1H NMR experiments useless at low temperatures.

3.2. X-ray crystallography

The molecular structures of compounds **1** and **3**–**5** are shown in Figs. 2–5. The crystalline compound **4·H₂O** shows disorder in two piperidine groups (Fig. 4). In this case, the H(C) atom positions were calculated and the hydrogen atoms were refined in isotropic approximation in the riding model with U_{iso}(H) parameters equal to 1.2 U_{eq}(Ci), 1.2 U_{eq}(Ni) and 1.2 U_{eq}(Oi), where U(Ci), U(Ni) and U(Oi) are the equivalent thermal parameters of the carbon, nitrogen and oxygen atoms, respectively, to which the corresponding hydrogen atoms are bonded. One of the piperidine rings in each independent molecule is disordered over two positions with relative occupancies 0.75/0.25. The atoms N(1) and N(1′) are common for both components. The occupancy of the minor component (0.25) is too low to refine the corresponding atoms in an anisotropic approximation. Hence, these atoms were refined isotropically.

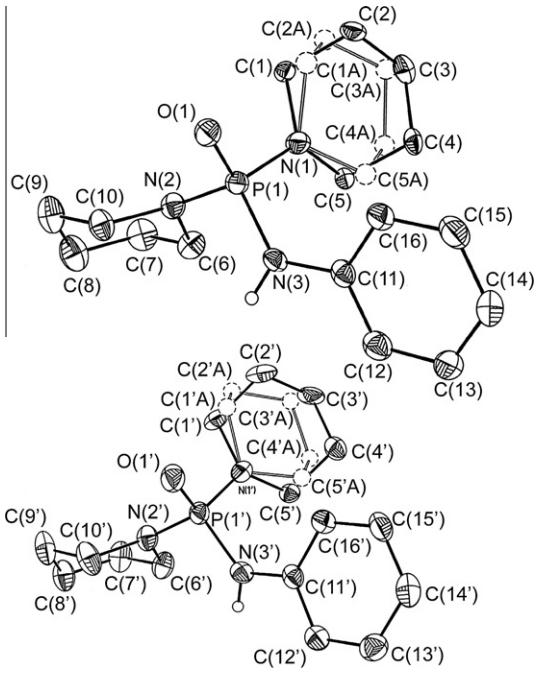

Fig. 4. Thermal ellipsoids (at the 50% probability level) of two conformers **4a** (a) and **4b** (b).

Selected bond lengths are given in Table 3. The mean P═O distances fall in the range 1.475–1.478 Å. This shows that the *para* substituent (X) of aniline does not significantly affect the P═O bond length. On the other hand, the mean P–$N_{aromatic}$ distance decreases from 1.657 (**1**) to 1.646 Å (**5**) in line with increasing the electron donation ability of the substituent X. It can be attributed to the charge donation of the methyl group to the phenyl ring. As a result, the participation of the nitrogen atom in the P–N bond is expected to be more than the nitrogen atom in the N–$C_{aromatic}$ bond. In the compounds **1** and **3**–**5**, the P═O bond and the phenyl ring take a gauche conformation with a torsion angle φ (Fig. 6 and Section 3.3.1). Rotation of the aniline and piperidine rings around the P–N bonds creates various conformers (Figs. 3–5).

Compound **1** contains only one conformer. In the crystal lattice of **1**, one-dimensional zigzag polymeric chains are produced by the N–H···O_P (O_P stands for phosphoryl oxygen atom) hydrogen bonds. Compound **3** contains four conformers **3a**, **3b**, **3c** and **3d** in the solid state. These conformers create two types of polymeric chains with **–(3a···3d···3c···3b)**$_n$– and **–(3a···3b···3c···3d)**$_n$– arrangements in the lattice (Fig. 7). Thus, the crystalline network of compound **3** includes of four types of hydrogen bond. Compound **4·H₂O** is composed of two conformers (**4a** and **4b**) and one water molecule in the solid state. The extended hydrogen bonds are formed due to the presence of H_2O in the unit cell. The water molecules connect the polymeric chains to produce double strands in the crystalline network of **4·H₂O**, as indicated in Fig. 8. Two zigzag chains with **–(5a···5c···5b···5d)**$_n$– and **–(5a···5d···5b···5c)**$_n$– arrangements are also created in the crystal lattice of compound **5**. This means that four types of hydrogen bond are established among the conformers.

It seems that the conformational diversity may change the crystal system of the compounds. The symmetry of the unit cell decreases with increase in the multiplicity of conformers. Accordingly, compound **1** crystallizes in the monoclinic crystal system with space group $P2_1/c$, while the crystals of compounds **3**, **4·H₂O** and **5** belong to the triclinic system and the space group $P\bar{1}$.

In the following sections we describe the structural and electronic features of the hydrogen bonds of the crystalline compounds **1**, **3**, **4·H₂O** and **5**. The hydrogen bond data of the compounds are given in Table 4. These hydrogen bonds display different donor–acceptor distances. It is noteworthy that strong hydrogen bonds are established in these compounds with donor–acceptor distances in the range 2.724–3.000 Å. The substituent X does not participate directly in hydrogen bonding. Also, it is not close enough to the phosphoryl group, hence no regular correlation can be found between the electronic nature of the substituent X and the strength of the intermolecular hydrogen bonds.

Conformers **4a** and **4b** are very close to each other from a structural point of view. They are different in their P═O bond length. The phosphoryl group of **4b** produces only the (**4a**)N–H···O_P(**4b**) hydrogen bond, while in the case of **4a** it is involved in two different hydrogen bonds (**4b**)N–H···O_P(**4a**) and O_W–H···O_P(**4a**) (O_W stands for the water oxygen atom) (Fig. 8). This may lead to increase the P═O bond length from 1.471(2) Å in **4b** to 1.486(2) Å in **4a**. The **4a**···**4b** hydrogen bond in compound **4·H₂O** is relatively weaker than those in the other compounds (Table 4). This may explain why compound **4·H₂O** has the lowest melting point in comparison with the others. It should be noted that the presence of a co-crystallized water molecule in the crystal lattice is another feature that may influence the melting point of compound **4·H₂O**.

3.3. NBO and AIM analyses

3.3.1. Fully optimized monomers in the gas phase

In order to investigate the effect of the *para* substituent of aniline on the electronic nature of the phosphoryl group, all compounds **1**–**5** have been separately modelled as single molecules in the gas phase. In all cases, a gauche configuration between the P═O bond and the phenyl ring is stabilized by the weak intramolecular CH···O_P hydrogen bond between the *ortho*-proton of aniline and the phosphoryl oxygen atom. This intramolecular contact creates a six-membered ring via O–P–N–C–C–H bond paths (Fig. 6). The NBO analysis reveals a weak electronic delocalization between the lone pair of the phosphoryl oxygen, Lp(O_P), and the vacant σ^*(C–H_{ortho}) orbital. Stabilization energies E^2 of 0.97, 0.86, 0.79, 0.83 and 0.79 kcal/mol^{-1} were obtained for the Lp(O_P) → σ^*(C–H_{ortho}) interaction in the compounds **1**, **2**, **3**, **4** and **5**, respectively. At the same level, AIM analysis reveals charge density (ρ) values at the bcp of the CH···O_P contacts in the range 0.0101–0.0110 a.u. for compounds **1**–**5**. The ρ values at the ring critical point (rcp) for the aforementioned six-membered ring (Fig. 9) vary from 0.0088 to 0.0093 a.u. in compounds **1**–**5**. Although these values are relatively small, they confirm the formation of weak intramolecular CH···O_P contacts. It is worthy to note that the ρ value at the rcp of the phenyl ring remains approximately unchanged by the replacement of the *para* substituent X. These bcps and rcps are illustrated in Fig. 9 and listed in Table 5.

The bond lengths, NBO charges, dipole moments, AIM parameters and the P═O stretching frequencies are listed in Table 5 for the fully optimized monomers **1**–**5** in the gas phase. The results show that the substituent X has no significant effect on the geometry and electronic features of the molecule. It has been previously described that the strength of inter-unit interactions in phosphoryl containing compounds is governed by the quantity of negative charge localized on O_P, $q(O_P)$ [9]. Here $q(O_P)$ does not change significantly with the *para*-substitution of the aniline. Thus, no difference is expected to create hydrogen bonds for the monomers **1**–**5**.

The Lp($N_{aniline}$) → σ^*(P–$N_{aliphatic}$) electronic delocalization weakens the P–$N_{aliphatic}$ bond. The stabilization energies E^2 of the Lp($N_{aniline}$) → σ^*(P–$N_{aliphatic}$) interaction are 9.41, 9.27, 9.11,

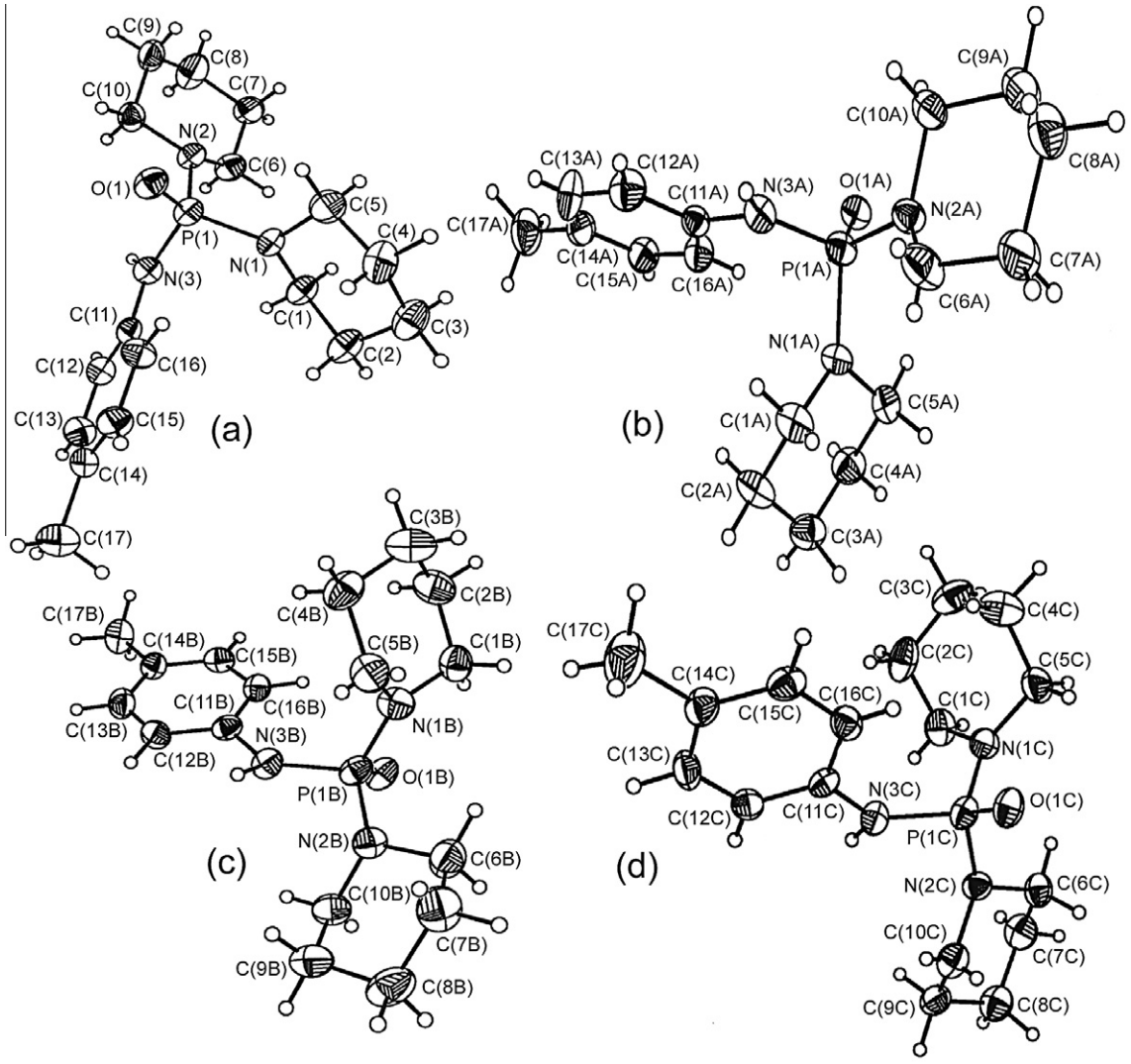

Fig. 5. Thermal ellipsoids (at the 50% probability level) of four conformers **5a** (a), **5b** (b), **5c** (c) and **5d** (d).

Table 3
Selected bond lengths (Å) and angles (°) for compounds **1** and **3**–**5**.

1		**3**		**4·H$_2$O**		**5**	
P(1)–O(1)	1.4786(15)	P(1)–O(1)	1.475(5)	P(1)–O(1)	1.486(2)	P(1)–O(1)	1.474(2)
P(1)–N(1)	1.6571(18)	P(1A)–O(1A)	1.469(5)	P(1′)–O(1′)	1.471(2)	P(1A)–O(1A)	1.475(2)
P(1)–N(2)	1.6495(18)	P(1B)–O(1B)	1.483(5)	P(1)–N(1)	1.644(2)	P(1B)–O(1B)	1.479(2)
P(1)–N(3)	1.6407(18)	P(1C)–O(1C)	1.471(5)	P(1′)–N(1′)	1.651(3)	P(1C)–O(1C)	1.476(2)
N(1)–C(1)	1.415(3)	P(1)–N(1)	1.648(6)	P(1)–N(2)	1.654(3)	P(1)–N(1)	1.634(3)
N(2)–C(7)	1.474(3)	P(1A)–N(1A)	1.654(6)	P(1′)–N(2′)	1.641(3)	P(1A)–N(1A)	1.641(3)
N(2)–C(11)	1.473(3)	P(1B)–N(1B)	1.646(6)	P(1)–N(3)	1.644(3)	P(1B)–N(1B)	1.638(3)
F(1)–C(4)	1.369(2)	P(1C)–N(1C)	1.659(6)	P(1′)–N(3′)	1.654(3)	P(1C)–N(1C)	1.632(3)
O(1)–P(1)–N(1)	113.58(9)	O(1)–P(1)–N(1)	112.7(3)	O(1)–P(1)–N(1)	110.94(12)	O(1)–P(1)–N(1)	111.59(14)
O(1)–P(1)–N(2)	110.99(9)	O(1A)–P(1A)–N(1A)	112.7(3)	O(1′)–P(1′)–N(1′)	111.96(14)	O(1A)–P(1A)–N(1A)	111.26(13)
O(1)–P(1)–N(3)	111.13(9)	O(1B)–P(1B)–N(1B)	112.5(3)	O(1)–P(1)–N(2)	109.79(12)	O(1B)–P(1B)–N(1B)	109.67(14)
N(1)–P(1)–N(2)	104.91(9)	O(1C)–P(1C)–N(1C)	112.8(3)	O(1′)–P(1′)–N(2′)	111.06(13)	O(1C)–P(1C)–N(1C)	109.98(15)
N(1)–P(1)–N(3)	106.34(9)	O(1)–P(1)–N(2)	117.8(3)	O(1)–P(1)–N(3)	116.45(13)	O(1)–P(1)–N(2)	110.77(14)
N(2)–P(1)–N(3)	109.58(9)	O(1A)–P(1A)–N(2A)	111.8(3)	O(1′)–P(1′)–N(3′)	113.91(14)	O(1A)–P(1A)–N(2A)	111.15(13)
C(1)–N(1)–P(1)	125.81(14)	O(1B)–P(1B)–N(2B)	117.9(3)	N(1)–P(1)–N(2)	109.64(14)	O(1B)–P(1B)–N(2B)	117.75(14)
C(1)–N(1)–H(1)	114.60(9)	O(1C)–P(1C)–N(2C)	111.5(3)	N(1′)–P(1′)–N(2′)	107.49(15)	O(1C)–P(1C)–N(2C)	117.61(14)
P(1)–N(1)–H(1)	116.80(9)	O(1)–P(1)–N(3)	109.9(3)	N(1)–P(1)–N(3)	104.51(13)	O(1)–P(1)–N(3)	113.63(14)
C(7)–N(2)–C(11)	112.69(17)	O(1A)–P(1A)–N(3A)	111.0(3)	N(1′)–P(1′)–N(3′)	105.53(13)	O(1A)–P(1A)–N(3A)	113.29(13)
C(7)–N(2)–P(1)	116.61(14)	O(1B)–P(1B)–N(3B)	110.2(3)	N(3)–P(1)–N(2)	105.17(13)	O(1B)–P(1B)–N(3B)	112.64(13)
C(11)–N(2)–P(1)	122.30(13)	O(1C)–P(1C)–N(3C)	111.0(3)	N(3′)–P(1′)–N(2′)	106.47(14)	O(1C)–P(1C)–N(3C)	113.31(14)

9.68 and 9.59 kcal/mol in compounds **1**, **2**, **3**, **4** and **5**, respectively. Thus, the amine groups can rotate similarly around the P–$N_{aliphatic}$ bond in all cases. It is found that the formation of various conformers in these compounds is independent of the electronic

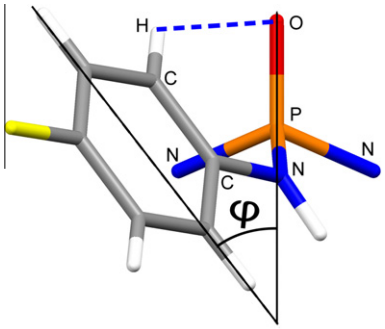

Fig. 6. Schematic representation of the gauche configuration for the P=O bond and phenyl ring. The intramolecular $CH_{ortho}\cdots O_P$ hydrogen bond is shown by a dashed line and the piperidine rings are reduced to their nitrogen atoms for clarity.

nature of the substituent X. Perhaps the steric effects play a dominant role in the formation of various conformers. Although the substituent X does not participate directly in hydrogen bonding, the crystal packing of the compounds is changed by the size of the substituents. Bulky substituents may affect the molecular arrangements in the hydrogen bonding. As a result, various conformers are created during the crystal growth. It is found that compounds **3** and **5**, with the bulky substituents $-CH_3$ and –Br, have four conformers in the solid state. The compounds with the small substituents –H and –F show no tendency to produce multiple conformers. It should be noted that the conformers **4a** and **4b** were converted to the equivalent structures, from energy and structural points of view, upon full optimization in the gas phase (Table 5). The observed conformational variety of compound **4·H$_2$O** can be attributed to the co-crystallization of the water molecule in the crystal lattice.

3.3.2. Comparison of the optimized monomers and clusters

For the compound **4·H$_2$O**, the modelled cluster contains **4a**, **4b** and water molecules, while triplet clusters were considered for the other compounds (Fig. 1). The donor–acceptor distances for the hydrogen bonds in the model clusters are equal to the experimental values, due to the freezing of the non-hydrogen atoms in the calculations. The other optimized parameters of the hydrogen bonds differ from the X-ray values (Table 4).

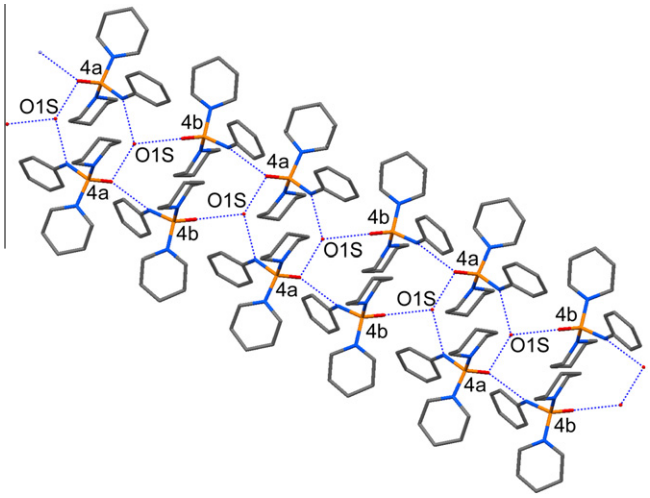

Fig. 8. A double strand created by molecules **4a**, **4b** and H_2O in the crystal lattice of **4·H$_2$O**. The symbol O1S refers to the oxygen atom of the water molecule.

A comparison of the fully optimized monomers and the hydrogen bonded clusters in the gas phase reveals that the intermolecular hydrogen bonding is responsible for the lengthening of the N–H bonds in clusters. This may explain the red shift of the N–H stretching frequencies from the calculated values to the experimental spectra. NBO analysis reveals an $[Lp(O_P) \rightarrow \sigma^*(N–H)]$ interaction among the subunits within the clusters. This electronic delocalization leads to the weakening of the N–H bond. This is in good agreement with the decrease in the ρ value at the bcp of the N–H bond from the monomers to their corresponding clusters (Tables 4 and 5). In all cases, the DH···A distances shorten from the X-ray data to the values derived from the DFT calculations. Moreover, the D–H–A angles in the optimized clusters are more linear than those in the solid state structures. These indicate that the hydrogen bonds in the optimized clusters are stronger than those in the X-ray structures. It is observed that the charge density at the bcp of DH···A is increased when the donor–acceptor distance shortens. The maximum ρ value is 0.0369 a.u. for the strongest hydrogen bond, i.e. $(HOH)\cdots O_P$(**4b**), while it is 0.0215 a.u. in the case of the **4b**$(NH)\cdots(O_P)$**4a** hydrogen bond with the

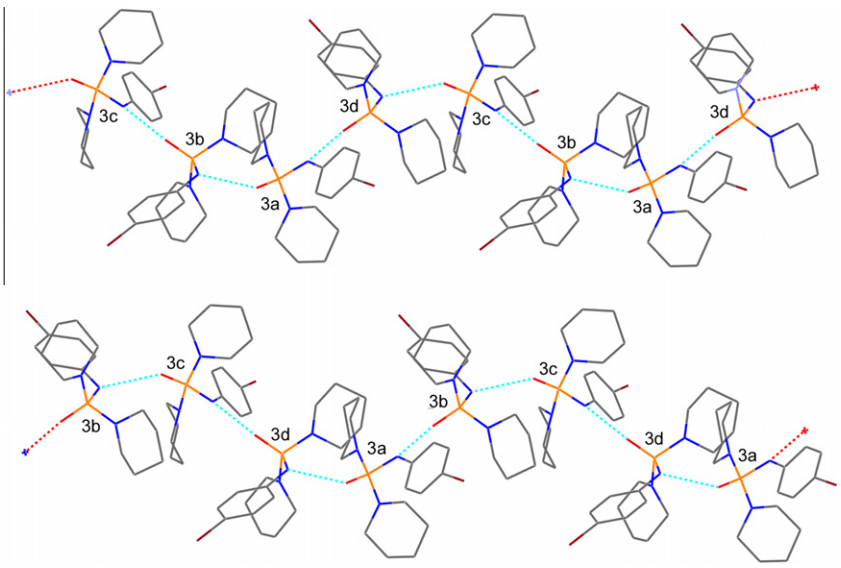

Fig. 7. Representation of two polymeric chains with $-(\mathbf{3a3d3c3b})_n-$ and $-(\mathbf{3a3b3c3d})_n-$ arrangements in compound **3**.

Table 4
The data[a] of the hydrogen bonds in the crystalline compounds.

D–H...A	D–A	d(D–H) Å	d(H···A) Å	d(D–A) Å	∠DHA°	SE[l]	ρ[m] (a.u.)	
							bcp1	bcp2
N(1)–H(1)···O(1)[b]	**1**···**1**	0.958 [1.022]	1.908 [1.847]	2.859(2)	171.6 [170.1]	[18.31]	[0.0318]	[0.0299]
N(1)–H(1)···O(1A)[c]	**3a**···**3b**	0.880 [1.023]	2.068 [1.855]	2.862(9)	149.6 [167.4]	[19.85]	[0.0316]	[0.0304]
N(1A)–H(1A)···O(1B)[d]	**3b**···**3c**	0.880 [1.026]	2.034 [1.813]	2.819(8)	148.0 [166.1]	[22.41]	[0.0314]	[0.0340]
N(1B)–H(1B)···O(1C)[e]	**3c**···**3d**	0.880 [1.024]	2.041 [1.861]	2.873(8)	157.0 [169.1]	[19.36]	[0.0316]	[0.0298]
N(1C)–H(1C)···O(1)[f]	**3d**···**3a**	0.880 [1.024]	2.005 [1.800]	2.807(8)	150.9 [166.7]	[22.89]	[0.0315]	[0.0347]
N(3)–H(3)···O(1S)[g]	**4a**···H_2O	0.870 [1.021]	1.979 [1.830]	2.842(3)	171.2 [170.3]	[20.19]	[0.0319]	[0.0341]
O(1S)–H(1S)···O(1')[g]	H_2O···**4b**	0.820 [0.978]	1.911 [1.752]	2.724(3)	170.8 [171.6]	[18.00]	[0.0331]	[0.0369]
O(1S)–H(2S)···O(1)[h]	H_2O···**4a**	0.820 [0.977]	2.023 [1.833]	2.808(3)	160.3 [176.3]	[15.19]	[0.0324]	[0.0327]
N(3')–H(3')···O(1)[i]	**4b**···**4a**	0.871 [1.020]	2.136 [2.000]	3.000(3)	171.8 [165.9]	[10.59]	[0.0319]	[0.0215]
N(3)–H(3N)···O(1C)[g]	**5a**···**5d**	0.900 [1.024]	2.045 [1.848]	2.854(2)	149.1 [166.3]	[19.90]	[0.0315]	[0.0311]
N(3A)–H(3NA)···O(1B)[g]	**5b**···**5c**	0.976 [1.024]	1.863 [1.820]	2.829(2)	169.7 [167.4]	[21.69]	[0.0315]	[0.0331]
N(3B)–H(3NB)···O(1)[j]	**5c**···**5a**	0.924 [1.024]	2.007 [1.904]	2.911(2)	165.4 [166.9]	[17.01]	[0.0316]	[0.0274]
N(3C)–H(3NC)···O(1A)[k]	**5d**···**5b**	0.938 [1.024]	1.962 [1.869]	2.880(2)	165.5 [168.7]	[19.12]	[0.0316]	[0.0295]

[a] The values in brackets refer to the optimized clusters at the B3LYP/6-31G* level.
[b] [x, $-y+1/2$, $z+1/2$].
[c] [x, $y-1$, z].
[d] [$-x+1$, $-y+3$, $-z+1$].
[e] [$-x$, $-y+3$, $-z+1$].
[f] [$x-1$, $y+1$, $z+1$].
[g] [x, y, z].
[h] [$-x$, $-y+1$, $-z$].
[i] [$x+1$, y, z].
[j] [$-x+1$, $-y+1$, $-z+1$].
[k] [$-x+1$, $-y+1$, $-z$].
[l] SE is the stabilizing energy E^2 (in kcal mol^{-1}) of the Lp(O) → σ*(N–H) and Lp(O) → σ*(O–H) delocalization effects.
[m] ρ is the calculated charge density at the bcps of the D–H bond (bcp1) and H···A contact (bcp2) in the cluster.

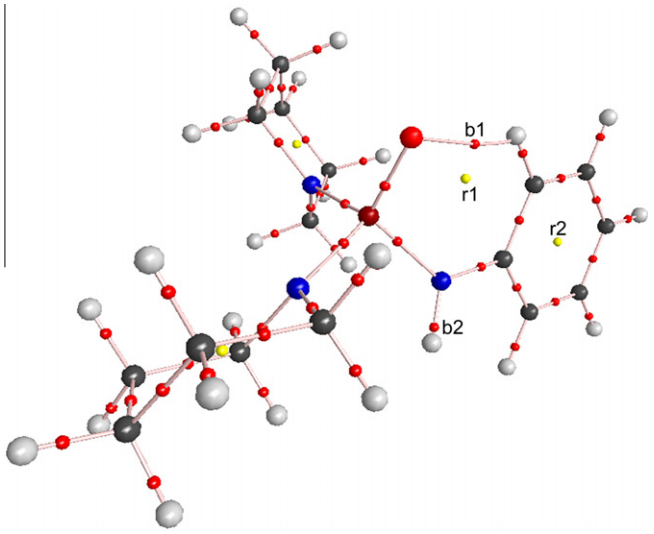

Fig. 9. Representation of the important bcp's and rcp's in the fully optimized monomer **4**.

longest donor–acceptor distance (3.000 Å). Coincident with this observation, a stabilizing energy E^2 of 18.00 kcal/mol^{-1} was calculated for the Lp(O_P) → σ*(O–H) delocalization effect of the (HOH)···O_P(**4b**) hydrogen bond, while it is 10.59 kcal/mol^{-1} in the case of **4b**(NH)···(O_P)**4a**.

4. Conclusions

The NMR data (at 298 and 190 K) confirm that the titled compounds have one conformer in solution. The crystal structures of **3**, **4**·**H$_2$O** and **5** contain four, two and four conformers, respectively, at 120 K. Rotation of the amine groups around the P–N bonds creates various conformers and a wide range of different hydrogen bonds. The N–H stretching frequency shows a red shift from the calculated to the experimental values, as a result of the packing effects in the solid phase. The $q(O_P)$ and $q(H_{amidic})$ values do not change upon *para*-substitution of the aniline. The conformational diversity in these compounds is independent of the electronic effects, and it is governed by steric effects, for example compounds **3** and **5**, with bulky substituents, produce four conformers in the solid phase.

Table 5
Selected bond lengths (Å), stretching frequencies (cm^{-1}), dipole moments (debye), NBO charges (e$^-$) and charge densities (a.u.) for the model monomers.

Compound	d(P=O)	d(N–H)	ν(P=O)	ν(N–H)	$q(O_P)$	$q(H_{amidic})$	Dipole moment	SE[a]	ρ[b]			
									(b1)	(b2)	(r1)	(r2)
1	1.490	1.012	1235	3604	−1.102	0.437	5.3	9.41	0.0107	0.3281	0.0090	0.0201
2	1.490	1.012	1235	3602	−1.101	0.436	5.6	9.27	0.0110	0.3282	0.0092	0.0202
3	1.489	1.012	1236	3602	−1.100	0.437	5.7	9.11	0.0109	0.3282	0.0093	0.0203
4	1.489	1.012	1236	3597	−1.101	0.436	4.4	9.68	0.0104	0.3281	0.0089	0.0201
5	1.490	1.012	1235	3602	−1.102	0.436	4.2	9.59	0.0101	0.3281	0.0088	0.0202
4a[c,d]	1.493	1.013	1229	3587	–	–	4.4	–	–	–	–	–
4b[c,d]	1.493	1.013	1229	3587	–	–	4.4	–	–	–	–	–

[a] SE is the stabilizing energy E^2 (in kcal mol^{-1}) of Lp($N_{aniline}$) → σ*(P–$N_{aliphatic}$).
[b] (b1) and (r1) are related to the bcp and rcp of the intramolecular CH···OP contact, (b2); bcp of the N–H bond, (r2); rcp of the aniline ring.
[c] The values are related to the B3LYP/6-31+G*level.
[d] The single point energy of conformer **4a** (−1206.28 HF) is equal to that of **4b** in the gas phase.

Acknowledgment

Support of this work by Tarbiat Modares University is gratefully acknowledged.

Appendix A. Supplementary data

CCDC 612549, 292746, 612550 and 612551 contain the supplementary crystallographic data for $C_{16}H_{25}FN_3OP$, $C_{16}H_{25}BrN_3OP$, $C_{32}H_{54}N_6O_3P_2$ and $C_{17}H_{28}N_3OP$. These data can be obtained free of charge via http://www.ccdc.cam.ac.uk/conts/retrieving.html, or from the Cambridge Crystallographic Data Centre, 12 Union Road, Cambridge CB2 1EZ, UK; fax: (+44) 1223-336-033; or e-mail: deposit@ccdc.cam.ac.uk.

References

[1] M.J. Dominguez, C. Sanmartin, M. Font, J.A. Palop, S.S. Francisco, O. Urrutia, F. Houdusse, J.M. Garsia-Mina, J. Agric. Food Chem. 56 (2008) 3721.
[2] G.L. Creason, M.R. Schmitt, E.A. Douglass, L.L. Hendrickson, Soil Biol. Biochem. 22 (1990) 209.
[3] R.K. Andrews, A. Dexter, R.L. Blakeley, B. Zerner, J. Am. Chem. Soc. 108 (1986) 7124.
[4] K. Gholivand, Z. Shariatinia, K. Khajeh, H. Naderimenesh, J. Enzym. Inhib. Med. Chem. 21 (2006) 31.
[5] J.C. Bollinger, J. Levy-serpier, J. Debord, B. Penicaut, J. Enzym. Inhib. Med. Chem. 3 (1990) 211.
[6] S.E. Denmark, S.M. Pham, R.A. Stavenger, X. Su, K.T. Wong, Y. Nishigaichi, J. Org. Chem. 71 (2006) 3904.
[7] S.E. Denmark, J. Fu, J. Am. Chem. Soc. 123 (2001) 9488.
[8] S.E. Denmark, R.A. Stavenger, K.T. Wong, Tetrahedron 54 (1998) 10389.
[9] K. Gholivand, H.R. Mahzouni, M.D. Esrafili, Theor. Chem. Acc. (2010), doi:10.1007/s00214-010-0743-5.
[10] D.E.C. Corbridge, Phosphorus, an Outline of its Chemistry, Biochemistry and Technology, fifth ed., Elsevier, Amsterdam, 1995.
[11] K. Gholivand, A.M. Alizadehgan, S. Arshadi, A.A. Firooz, J. Mol. Struct. 791 (2006) 193.
[12] K. Gholivand, M. Pourayoubi, Z. Anorg. Allg. Chem. 630 (2004) 1330.
[13] K. Gholivand, M. Pourayoubi, M.D. Alavi, Z. Kristallogr, NCS 219 (2004) 124.
[14] K. Gholivand, Z. Shariatinia, M. Pourayoubi, Z. Naturforsch. B 60 (2005) 67.
[15] M.J. Cain, A. Cawley, V. Sum, D. Brown, M. Thornton-Pett, T.P. Kee, Inorg. Chim. Acta 345 (2003) 154.
[16] K. Gholivand, H. Mostaanzadeh, T. Koval, M. Dusek, M.F. Erben, C.O.D. Vedova, Acta Crystallogr., Sect. B 65 (2009) 502.
[17] K. Gholivand, C.O.D. Vedova, A.A. Firooz, A.M. Alizadehgan, M.C. Michelini, R.P. Diez, J. Mol. Struct. 750 (2005) 64.
[18] K. Gholivand, Z. Shariatinia, M. Pourayoubi, Polyhedron 25 (2006) 711.
[19] R.E. Babine, S.L. Bender, Chem. Rev. 97 (1997) 1359.
[20] S. Liu, G.L. Gilliland, W.J. Stevens, R.N. Armstrong, J. Am. Chem. Soc. 115 (1993) 7910.
[21] T. Steiner, G. Koellner, J. Mol. Biol. 305 (2001) 535.
[22] A.N. Pankratov, A.V. Shalabay, J. Struct. Chem. 48 (2007) 427.
[23] Bruker, SMART, Bruker Molecular Analysis Research Tool, v. 5.059. Bruker AXS, Madison, Wisconsin, USA, 1998.
[24] G.M. Sheldrick, SHELXTL v. 5.10, Structure Determination Software Suite, Bruker AXS, Madison, WI, USA, 1998.
[25] G.M. Sheldrick, In: SADABS v. 2.01, Bruker/Siemens Area Detector Absorption Correction Program, Bruker AXS, Madison, WI, USA, 1998.
[26] K. Gholivand, S. Ghadimi, H. Naderimanesh, A. Forouzanfar, Magn. Reson. Chem. 39 (2001) 684.
[27] A.E. Reed, L.A. Curtiss, F. Weinhold, Chem. Rev. 88 (1988) 899.
[28] R.F.W. Bader, Atoms in Molecules: A Quantum Theory, Oxford University Press, Oxford, UK, 1990.
[29] R.F.W. Bader, Chem. Rev 91 (1991) 893.
[30] M.J. Frisch, G.W. Trucks, H.B. Schlegel, G.E. Scuseria, M.A. Robb, J.R. Cheeseman, V.G. Zakrzewski, J.A. Montgomery Jr., R.E. Stratmann, J.C. Burant, S. Dapprich, J.M. Millam, A.D. Daniels, K.N. Kudin, M.C. Strain, O. Farkas, J. Tomasi, V. Barone, M. Cossi, R. Cammi, B. Mennucci, C. Pomelli, C. Adamo, S. Clifford, J. Ochterski, G.A. Petersson, P.Y. Ayala, Q. Cui, K. Morokuma, D.K. Malick, A.D. Rabuck, K. Raghavachari, J.B. Foresman, J. Cioslowski, J.V. Ortiz, A.G. Baboul, B.B. Stefanov, G. Liu, A. Liashenko, P. Piskorz, I. Komaromi, R. Gomperts, R.L. Martin, D.J. Fox, T. Keith, M.A. Al-Laham, C.Y. Peng, A. Nanayakkara, C. Gonzalez, M. Challacombe, P.M.W. Gill, B. Johnson, W. Chen, M.W. Wong, J.L. Andres, C. Gonzalez, M. Head-Gordon, E.S. Replogle, J.A. Pople, GAUSSIAN98, Revision A.7, Gaussian Inc., Pittsburgh, PA, 1998.